Xiang, J., Heng, J., & New, T. H. (2017). A numerical parametric and optimization study of an industrial air-slide conveyor system. Powder Technology, 315, 367–378.

A numerical parametric and optimization study of an industrial air-slide conveyor system

Junting Xiang[+], J. Heng and T. H. New*

School of Mechanical and Aerospace Engineering
Nanyang Technological University, 50 Nanyang Avenue
Singapore 639798

Abstract

A numerical investigation has been conducted to model the cement flow behaviour associated with a full-scale industrial air-slide conveyor (ASC) system. Steady-state simulations on the ASC were performed to predict its operational and the cement flow characteristics, and comparisons with actual operational data of the ASC demonstrate satisfactory agreement. Subsequently, hopper input loading, velocity as well as the suction fan pressure were varied and simulated to identify how cement conveying capacity by the ASC may be increased. Simulation results indicate that an increase in air chamber pressure leads to a corresponding increase in conveying capacity because of the enhanced capability of air chamber to sustain the cement flow, whereas increasing hopper input velocity and suction fan pressure both lead to lower demands in the air chamber pressure required to sustain existing conveying capacity. Detailed results associated with the cement and air flow mixture behaviour within the ASC reveal that, while the cement and air mixture flow is highly complex and three-dimensional, gross trends between the various operational parameters can be isolated successfully and may offer insights into how the existing ASC may be modified to increase conveying capacity.

Keywords: Pneumatic conveying system; air-slide conveyor; numerical simulations; cement transportation; two-phase flow

[+] Presently at School of Engineering, Deakin University, Geelong, Australia

* Corresponding author – dthnew@ntu.edu.sg; Tel – +(65) 6790 5130

1. Introduction

1.1 Research background

Due to increased demand for cement powder in the construction industry, greater attention is now being paid towards optimizing its delivery throughout the entire logistical chain. For regions where shortages in local cement production are being faced, the cement is typically transported from the place of origin via bulk marine vessels from port to port. Upon the arrival of these bulk vessels at their ports-of-call, the cement is commonly offloaded through shore side screw unloaders to the hopper systems via pneumatic conveying pipes, before the cement is transported to the storage silos via the pneumatic air-slide conveying systems. It should be noted that a pneumatic based delivery process is one of the most efficient ways to transport powdery materials and hence, it should not come as a surprise that it is a well-accepted and common practice to transport cement and other different powdery or granular materials [1, 2].

1.2 Literature review

To better understand and improve the operations associated with various components associated with pneumatic conveying systems, experiments and numerical studies have been conducted previously to isolate the key conveying characteristics [3, 4]. Take for instance, Li et al. [3] numerically studied the effects of material properties on horizontal pneumatic conveying based on discrete element method, and observed that friction and restitution coefficients of particles affect particle velocity, solid concentration and pressure drop, amongst others. Yan et al. [5] measured particle velocity and concentration distributions using high-speed particle image velocimetry (PIV) technique to look into the conveying velocity and pressure drops in a soft-fin based self-excited horizontal pneumatic conveying. Additionally, Gupta et al. [6] made use of a 3.7 meter long fluidized conveying system to

investigate dry particulate material transportation behaviour at different conveyor inclinations. The resulting increases in air velocity were found to lead to increases in the material mass flow rate, and the material mass flow rate tends to decrease when the conveying orientation varies from downwards to upwards direction.

Mittal et al. [7] studied the flow mechanisms associated with the pneumatic conveying of fine powders conveyed from fluidized dense phase to dilute phase. Different signal analysis techniques were also applied to pressure fluctuation results, from which the nature of the flows within the pipelines was revealed. Pu et al. [8] incorporated a kinetic-friction model into the two-fluid model in their numerical study of dense phase pneumatic conveying of pulverized coal, where the simulations predicted pressure gradients and solid concentration distributions that agreed well with experimental results. Other parameters such as particle fluctuation velocity [9], particle agglomeration [10], solid friction factor [11], wall roughness induced secondary flow [12], and more research into pneumatic conveying systems can be found in other experimental/numerical studies [13-17]. In particular, it is worthwhile to highlight that numerical simulations are able to capture the most important characteristics associated with powdery flows successfully, despite some of the limitations faced in modelling particle dynamics.

1.3 Research significance

The large-scale nature of industrial pneumatic conveying systems naturally implies that full-scale experiments and numerical simulations of the entire cement transport behaviour from the port side all the way to the silo is daunting, cost-ineffective and impractical. In particular, it should be noted that numerical simulations require adequately small mesh cell size to resolve the cement flow behaviour properly, which clearly is an issue when it comes down to

modelling full-scale industrial pneumatic conveying systems. On the other hand however, it may be possible to do so for select components of the pneumatic conveying system, provided that a satisfactory compromise is struck between accuracy and computational resources. Hence, this leads to one of the primary motivations driving the present study. The second primary motivation stems from the desire to understand the relationships between the various operating parameters of a real-world industrial air-slide conveyor (i.e. ASC) for cement flows through a numerical study, so as to optimize its operations. In particular, the ASC in question here is one of two presently in operation at Jurong Port Pte Ltd (i.e. abbreviated as the operator hereafter), Singapore. It has to be highlighted that the operator is currently the only port-of-call in Singapore that handles cement powder via bulk vessels and its handling capacity directly affects the building and construction sector in Singapore.

An ASC system relies on pressurized air being injected into a lower chamber, from which the air will flow across a fabric and produce an air film for the cement powder to flow down the entire upper conveying chamber. To illustrate, Fig. 1 shows a schematic diagram of the industrial ASC system working process. It is generally used to transport the cement from the hopper system to the silos for storage purposes and its conveying capacity is influenced by the pressurized air pressure, upstream initial conditions, downstream exit conditions, downstream suction air pressure, inclination, physical geometry and behaviour of cement powder flows, just to name a few. While earlier studies might have look at selected sections or scaled-down of an ASC and provided useful insights, studying an actual industrial ASC system numerically with engineering data from the operator used for validation provides a rare opportunity to assess if state-of-the-art numerical simulations are able to predict industrial flow applications satisfactory. It is also worthwhile to mention that such operation data remains very limited in the open literature, due to potential concerns over proprietary

commercial information. Nevertheless, it will be seen later that bulk flow data provided by the operator are sufficient for validation and hence prediction purposes.

In the next few sections, the physical design and actual operational details associated with the industrial ASC system will be introduced. This will be followed by a description of the numerical procedures, input parameters and boundary conditions used in the simulations. Thereafter, numerical results from steady state simulations will be presented and discussed. In particular, relationships between the various operational parameters mentioned earlier and the cement transport rates when the former was varied will be discussed in detail, providing insights into how the operation of the ASC system may be potentially altered to increase overall cement transport rates.

2. Physical design and operational details of air-slide conveyor

The ASC currently used by the operator was designed to deliver cement from the hopper system to the storage silos. Due to the present operational conditions faced by the operator, the ability to transport cement to the silos by the ASC currently limits the maximum overall cement conveying speed from the bulk vessels. Key physical design details of the ASC are provided in Table 1. Firstly, the ASC comprises two separate upper and lower chambers, the former for cement conveying while the latter is where pressurized air is being injected. The two chambers are separated by a porous fabric. The ASC was installed with an inclination of $\beta=7°$ and there are a total of four separated lower air chambers with a 0.63m (W) × 0.07m (H) cross-section. Each air chamber is supplied with air from a central pump separately and no air crosses between the four air chambers. The first air chamber has a length of approximately 3m, with subsequent three air chambers having lengths of 30m each. In contrast, the upper

cement chamber is a continuous rectangular channel with a 0.63m (W) × 0.52m (H) cross-section.

Porous FLUITEX-E-800/5 fabric was used to separate the cement chamber from the air chamber, allowing pressurized air to pass through and form a fluidized bed for cement transportation. The current operating air pressures in the first and subsequent three air chambers are 7500Pa and 6000Pa respectively. In addition, a suction fan with a 2500Pa pressure drop was installed at the cement chamber exit to aid cement transportation. The air velocity through fabric is estimated to be 0.033m/s, where it was determined based on the air supplied under typical working conditions and fabric porous area. Lastly, the design operation capacity of the ASC is rated at C_o=800tons/hr under ideal conditions, assuming no significant cement input suspension occurs during operation. Fig. 2 shows a photo of the actual ASC and its dimensions.

3. Numerical simulation procedures

3.1 Geometry and mesh generation

Based on the physical geometries of the ASC, structured mesh based computational domains and meshes were generated for both the air and cement chambers and shown in Fig. 3. To simplify matters, x-axis refers to the streamwise direction, though it should be reminded that the ASC was installed with an inclination of 7^o . The y- and z-axes are along the width and height of the ASC respectively.

Note that the hopper exit (i.e. where cement begins to flow into the ASC) is located on top of the first cement chamber (i.e. see Fig. 3(a)) and possesses the same dimensions and location as the actual ASC. For the first cement chamber, the general cell sizes are 10mm along

streamwise and cross-stream of the cement flow direction. Along the cement chamber height direction, a growth ratio of 1.05 was applied with a total of 30 mesh cells, so to produce refined cells near the fabric surface to accommodate more intense interactions between the cement and pressurized air occurring there. The preceding mesh configuration was found to be a satisfactory compromise between simulation accuracy and computational time. The subsequent three cement chambers made use of similar mesh specifications to allow smooth transitions of the flow behaviour within the entire computational domain. Further downstream, a chamber exit with a suction fan was modelled at the end of the cement chamber in accordance to the actual ASC physical geometries, as shown in Fig. 3(b). To simplify the modelling and subsequent simulations, the air chamber was modelled as a uniform air flow into the cement chamber with a velocity of 0.033m/s through the fabric porous areas, as was approximated from the actual ASC. Hence, it can be seen from the preceding descriptions that the numerical model was based on the actual ASC dimensions and is a good representation of the actual operational conditions.

The mesh was created using Gambit 2.4 with a total of 17.8 million structured cells. The mesh quality was estimated using cell skewness and it was observed that 99.5% of the cells lie within a skewness range of 0 to 0.1, indicating good quality mesh had been created. This mesh is sufficiently fine to capture the cement flow characteristics satisfactorily, based on the mesh independent study carried out previously and the computational resources available.

3.2 Numerical procedures

The simulations were performed using ANSYS Fluent 13.0 solver, where initial and boundary conditions were defined according to the actual geometries, flow conditions and material properties. The hopper exit into the ASC was defined as a velocity inlet flow

condition with velocities ranging from 1m/s to 4m/s. The ASC exit was defined as a pressure outlet flow condition with pressure drops ranging from 0Pa to 6000Pa. The conveyor walls were defined as "no-slip" wall boundary conditions and the fabric area was defined using velocity inlet boundary conditions with a constant air velocity value of 0.033m/s. Stokes number St (defined as $St = (\rho_p d_p^2 U_0)/(18\mu L_0)$), commonly used to characterize suspended particle behaviour within fluid flows, was estimated to be S_t<<1 based on the physical geometries and operating flow conditions. As such, the particles would follow fluid streamlines closely [18]. A mixture model was used during the simulations, due to its capability in handling dispersed-phase flow and cost-effectiveness, computationally speaking.

The mixture model is a simplified Eulerian model that treats the phases as interpenetrating continua, solves the mixture momentum equation and prescribes the relative velocities of the dispersed phase. The following equations are the governing equations used in the mixture model:

Continuity equation:

$$\frac{}{\partial t}(\rho_m) + \nabla \cdot (\rho_m \vec{v}_m) = 0, \text{ and} \quad (1.1)$$

Momentum equation:

$$\frac{}{\partial t}(\rho_m \vec{v}_m) + \nabla \cdot (\rho_m \vec{v}_m \vec{v}_m) =$$

$$-\nabla p + \nabla \cdot [\mu_m(\nabla \vec{v}_m + \nabla \vec{v}_m^T)] + \rho_m \vec{g} + \vec{F} + \nabla \cdot (\sum_{k=1}^{n} \sigma_k \rho_k \vec{v}_{dr,k}\, \vec{v}_{dr,k}), \text{ and} \quad (1.2)$$

Energy equation:

$$\frac{}{\partial t}\sum_{k=1}^{n}(\sigma_k \rho_k E_k) + \nabla \cdot \sum_{k=1}^{n}\left(\sigma_k \vec{v}_k (\rho_k E_k + p)\right) = \nabla \cdot \left(k_{eff} \nabla T\right) + S_E \quad (1.3)$$

where $\vec{v}_m = \frac{\sum_{k=1}^{n} \sigma_k \rho_k \vec{v}_k}{\rho_m}$ is the mass-averaged velocity, $\rho_m = \sum_{k=1}^{n} \sigma_k \rho_k$ is the mixture density, σ_k is the volume fraction of phase k, n is the number of phases, $\vec{F}$ is a body force,

$\mu_m = \sum_{k=1}^{n} \sigma_k \mu_k$ is the viscosity of the mixture, $\vec{v}_{dr,k} = \vec{v}_k - \vec{v}_m$ is the drift velocity for the secondary phase k, k_{eff} is the effective conductivity and S_E includes any other volumetric heat sources.

The *k*-ε turbulence model was used for turbulence modelling, due to its simplicity and its well-established modelling capabilities. Gravitational force was enabled and the wall roughness was assumed to be negligible. Table 2 shows the various input parameters used for the present simulations. Conventional Portland cement was conveyed in the actual ASC and thus modelled here with a constant mean particle size of φ=14μm throughout the simulations [19]. Note that earlier studies have also observed that conventional Portland cement tends to have particles sizes ranging from 10 to 15μm as well [20-22]. To simplify the simulations, note that particle size variations [20, 21] and particle coagulations due to humidity were not taken into considerations for the steady-state simulations here.

To achieve that, a constant restitution coefficient of e=0.9 was defined, assuming the particle collisions were approximately elastic. It also guaranteed that the particle coagulations and the dissipation of particle kinetic energy were negligible. A bulk density of ρ_{bulk}=1362kg/m^3 was used for the cement here, according to its packing limit. The fluidized density was a function of both cement volume fraction and bulk density, while the combination of cement volume fraction and hopper velocity defined the mass flow rate and the expected operation capacity (C_o). The simulation boundary conditions were set to match the actual ASC operating conditions. In this case, the hopper velocity was defined as v_{hopper}=4m/s and the cement volume fraction was defined as V_f=0.15 to be consistent with C_o=836.68tons/hr industrial value. Besides that, a conveyor inclination of β=7° and a pressure drop at suction fan of 2500Pa were defined, identical with the actual ASC operating conditions.

4. Simulations and Results

4.1 Steady-state simulation of the ASC under operational conditions

Based on the above simulation settings, steady-state simulation of the actual air-slide conveyor was carried out and took approximately two weeks of computations with eighty processors to reach satisfactory convergence. Fig. 4 shows the computed pressure distributions along the ASC, where the four cement chambers are indicated. The first and last cement chambers are shown located on the top-left and bottom-right of the ASC figure respectively. The results indicate that a gradual decreasing pressure distribution exists from the hopper region within the first cement chamber towards the end of the last cement chamber. As such, it can be deduced that pressure gradient and gravitational forces are the primary driving forces behind the cement flow, as expected. Interestingly, a high pressure zone can also be identified in the first cement chamber ahead of the hopper region and postulated to be due to the presence of a slow-moving recirculating zone between the left-most wall of the first cement chamber and the hopper region.

To investigate in greater details, solid concentration distributions taken at different cross-sectional YZ planes (i.e. across the cement chambers) are presented in Fig. 5 to illustrate how the cement flow develops along the ASC. In this case, the solid concentration is defined as $S_c=\rho_{mixture}/\rho_{bulk}$ and seven different cross-sectional results taken between x=5m to 90m (i.e. from near hopper to near suction fan) are included in the figure. The red and orange regions represent relatively higher cement concentrations, while the blue region represents lower cement concentrations. In general, the solid concentration level decreases from x=5m to 90m, and indicates that a more dilute phase flow situation exists in the downstream region of the ASC. This also means a decreased fluidized density level towards the downstream of the ASC system due to its correlation with the solid concentration ($S_c=\rho_{mixture}/\rho_{bulk}$). In addition,

the decreased fluidized density leads to better mixture flowability and correlated with a lower pressure value towards the conveyor exit as shown in Fig. 4. On the other hand, variations in the solid concentration level become smaller in the downstream regions of the ASC, because of the well-diluted mixture phase in that region. It should be highlighted that in the early stages of the cement conveying, the air issuing through the fabric occasionally results in the cement detaching from the fabric surface significantly and contributes to the formation of vortices in the two-phase flow. As the cement flow develops further downstream however, a thin and more stable fluidized layer will form along the fabric surface, even though evidence of occasional vortex formations can still be observed.

To probe further and demonstrate how the flow may evolve within the different chambers, Fig. 6 shows velocity vector maps taken at x=5m, 45m and 90.5m, where large-scale flow motions are highlighted. Note that the plots are orientated such that the flows are moving towards the readers and that the velocity vectors are coloured according to the velocity magnitudes. To begin with, Fig. 6(a) shows the cross-sectional velocity vector field taken along x=5m location, where it is located shortly after the hopper region. Due to the cement entering into the chamber from the hopper, a pair of recirculating regions is formed close to the top chamber corners. The presence of these recirculating regions leads to flows moving upwards along the chamber walls and towards the top-corners. On the other hand, a small vortex is produced above the fabric surface due to the air pushing out from the fabric and encountering the sliding flow within the chamber. This and other vortices are expected to exert flow influences further downstream and introduce additional transient flow effects.

As the cement flows further downstream till x=45m as shown in Fig. 6(b), the pair of recirculating regions observed in Fig. 6(a) is no longer present. Instead, one large

recirculating region located at the bottom-right of the chamber is observed. Additionally, a small vortex can be seen just above the fabric surface on its left-hand side. These findings suggest that the cement flow along the ASC does not remain invariant and changes are expected as it travels along the rather significant ASC length. Lastly, at the exit of the ASC at x=90.5m as shown in Fig. 6(c), strong downwards acting velocity vectors can be detected and this is clearly due to the cement and air exiting out of the chamber, particularly under the actions of the suction fan. Despite this strong fluid flow action, there remain some evident corner flows along the top-corners of the chambers. These preceding results not only demonstrate just some of the drastic changes to the cement flow from the hopper to the ASC exit regions, but also highlight the surprising significant secondary flows that exist within the ASC, which are typically ignored in real-world operations.

It has been seen in Fig. 5 earlier that the solid concentration level remains higher closer to the fabric despite distribution variations between different cross-sectional planes. This can be better appreciated by the solid concentration levels taken at different distances away from fabric surface on x=45m plane (i.e. 20%, 30%, 40% and 50% of chamber height) and these locations are illustrated in Fig. 7 for clarity. Note that for this comparison, the legend of the solid concentration value is non-dimensionalized such that a maximum value of S_c=0.1 is specified to better present the variations. Also, it has to be highlighted that solid concentration distributions closer to the fabric surface were not used in this comparison, as the occasional vortex formations caused by the air passing through the fabric may dramatically affect the local cement distribution. Fig. 8(a) shows the distributions of solid concentration level and the results show that the cement particles tend to be located in the lower regions of the cement chamber. This is consistent with experimental observations made by past studies and that observed in the actual ASC at the operator site. While there are some

minor instances when solid concentration level is higher further away from the fabric surface, this can be attributed to the occasional transient interactions between the cement and air issuing from the fabric.

Fig. 8(b) shows the distribution of the bulk velocity U, which is defined as $U=(U_x^2+U_y^2+U_z^2)^{1/2}$. Firstly, it is interesting to note that the cross-sectional velocity distributions are not symmetrical, which again could be attributed to the transient nature of cement flowing down the ASC. But generally speaking, the trends are within expectations in the sense that mean velocities tend to be higher in the lower zone of cement chamber. As seen from Fig. 8(a) where more cement particles are shown to reside closer to the fabric surface, the value of the dominating X velocity component is less likely to be affected by the vortex triggered from fabric surface due to the higher momentum of cement flow in the lower zone. In contrast, the cement flow further away from fabric surface is more prone to be affected by the vortex and circulation zone as shown in Fig. 6(b), which results in a smaller velocity magnitude in the upper zone of cement chamber. It should be noted that the apparent viscosity of the cement-air mixture tends to decrease in the ASC downstream region. The apparent viscosity increases with respect to solid fraction, when lubrication forces between particles play an increasing role for higher solid fraction cases [23]. In the current simulations, the variation of apparent viscosity within the ASC system indicates higher apparent viscosity value and hence higher friction between particles in regions of higher solid fraction, which also indicates possibly higher temperature in those regions due to increased particle friction effects. Thus, while friction-induced temperature changes, humidity-induced particle aggregation issue as well as interaction between particles and fabric surface will contribute to the velocity magnitude distributions to some extent, the current simulations do not take these effects as a matter of simplifying the task of simulating the full-scale ASC system here.

Significant deviations of the velocity magnitude can be observed from y=0.1m onwards, but that is due to the formation of a corner vortex (see Fig. 7) close to the top-right region of the cement chamber. This will also explain the deviations in the solid concentration levels seen in the region in Fig. 8(a).

With cross-sectional variations in the solid concentration level and velocity clarified, Fig. 9 shows the velocity distributions along the entire ASC. Due to the significant ASC length, the results are separated into three distinct parts – first and second cement chamber, third chamber and then the last chamber, as indicated in Figs. 9(a), (b) and (c) respectively. As the cement enters the first chamber from the hopper, Fig. 9(a) shows that the bulk velocity gradually increases as the cement travels to the second cement chamber. Low-velocity regions exist in the first cement chamber, where they are mainly located before and after the hopper region – note that this has been observed in results presented earlier. This is due to the generation of an upstream recirculating region as a result of the cement leaving the hopper and the confined nature caused by the upstream wall of the first chamber. To better appreciate this recirculating region, its streamlines are plotted and presented in Fig. 10(a). Note that some flows associated with the recirculating flow eventually convey down the ASC under the actions of the higher speed flows close to the top of the chamber. As the cement exits from the second chamber and enters the third chamber, the bulk velocity continues to increase. Interestingly, flows close to the fabric surface show increasingly strong interactions between the cement particles and air exhausting from the fabric, producing larger velocity variations within this chamber onwards. This is particularly evident in the last one-third of the third chamber. Lastly, when the cement enters the last chamber as shown in Figs. 9(c) and 10(b), the bulk velocity increases further, though the general velocity distribution as viewed along this plane becomes more uniform as compared to Fig. 9(b). The flow is better developed and

the large velocity in these regions results in more diluted phase of cement flows, despite occasional vortex formations close to the fabric surface.

To summarize the preceding results, a declining trend of pressure distribution along the ASC is predicted, indicating that pressure gradient and gravitational force are the primary driving forces behind the cement flow behaviour. In addition, cement particles tend to be located at the lower regions of the cement flow chambers. Strong stochastic and turbulent flow patterns within the ASC system are predicted by the simulations and the predicted cement conveying rates agree well with that reported by the operator.

With baseline simulations established for the ASC in accordance to the working conditions employed by the operator, the effects of varying several key working conditions as derived from additional simulations will now be discussed.

4.2 Effects of cement mass flow rate

One of the most important parameters that any ASC operator is interested in will be the maximum cement mass flow rate transportable by the ASC, provided that the hopper system is not limited in the cement mass flow rate that it is able to dispense. However, it should also be mentioned that higher cement mass flow rates will naturally lead to higher cement volume fractions (i.e. denser phase flows) that are likely to introduce practical issues such as possibilities of flow choking. Hence, the present study offers a unique opportunity to look into the effects of key parameters upon the ASC operations. In this section, the effects of cement mass flow rate, particularly higher ones, on the overall flow behaviour within the cement chambers will be explored to see if the ASC is able to handle higher cement conveying rates. To simplify matters and reduce computational time however, only the first

and second cement chambers were considered during the simulations. For the simulations, the original cement exit velocity at the hopper remained unchanged at v_{hopper}=4m/s, while the cement volume fraction was varied from V_f=0.1 to 0.25. This resulted in cement mass flow rates ranging from 154.94kg/s to 387.35kg/s and corresponding operation capacities of C_o=557.78tons/hr to 1394.47tons/hr. These variations are detailed in Table 3 and all other initial and boundary conditions remain unchanged for the sake of consistency.

Fig. 11 shows the computed solid concentration level distributions along the first and second chambers of the ASC under different operating capacities. Note that the legend scales with the local maximum S_c for each test case to better highlight the flow behaviour. At C_o=557.78tons/hr where it is below the actual operating capacity, the cement granule is well fluidized and diffused with air for the most part within the second chamber. With the increase of operation capacity, higher solid concentration values are identified and the occurrence of slug flow is observed when it exceeds the operating capacity at operator site. Due to the more compacted nature of cement particles in the ASC for higher operation capacity cases, it will potentially lead to ASC stall when the humidity and cement particle friction effects are counted in.

To understand the requirements placed upon the air pressure within the air chamber and the general trend for the expected pressure increments to support higher operating capacities, Fig. 12 shows the relationship between air pressure in the first air chamber and the operating capacity. While there are only four data-points available from the present study, the almost linear trend between the two parameters within the range investigated here is surprisingly clear. Having said that, it has to be emphasized that the present simulation were performed without taking into consideration other factors such as humidity and particle size variations

due to the complexities of incorporating them. The results presented in Fig. 11 do show higher occurrences of cement agglomeration and slug flow patterns when the operating capacity is increased beyond the level currently used by the actual ASC at the operator site. The solid flow rate of the fluidized mixture plays a critical role in simulation, as it determines the conveying capacity of the system and largely impacts on flow patterns. Other Portland cement inherent properties such as specific surface area, particle size and chemical composition and so on, are assumed unchanged throughout the current simulation work. Incorporating these afore mentioned factors are likely to produce flow behaviour more severe than those shown in Fig. 11 and more realistic simulations will have to be conducted to go beyond the general trends identified here.

In summary, numerical results predict that the ASC cement conveying rate could be improved by increasing air chamber pressure. On the other hand, cement agglomeration and slug flow behaviour do manifest when the operating capacity goes beyond the current operating level of the ASC system.

4.3 Effects of cement exit velocity from the hopper

In this section, the role of cement exit velocity from the hopper will be examined and discussed. With the operation capacity fixed at C_o=836.68tons/hr, different combinations of cement volume fraction and hopper velocity are simulated to clarify their effects on the flow behaviour within the ASC. Similar to the previous section, all other initial and boundary conditions remained unchanged unless specified. Note that variations in the cement exit velocity would lead to corresponding changes to the other parameters such as cement volume fraction, as shown by the different combinations studied here listed in Table 4. Note that different cement volume fraction led to different fluidized density, while the cement exit

velocity was varied from 1m/s to 4m/s to maintain mass flow rate and operation capacity unchanged. The variations of cement exit velocity from the hopper were pre-determined by the shore side screw unloader to the hopper system through the pneumatic conveying system, where the overall cement mass flow rate will be controlled to align with the operator's handling capacity.

Fig. 13 shows the relationship between the first and second air chamber pressures and the cement exit velocity from the hopper. It can be readily appreciated that regardless of the exact air chamber, a lower air chamber pressure is required as the cement exit velocity increases. Physically speaking, this implies that faster moving cement exiting from the hopper requires less air issuing from the fabric to support its conveyance along the ASC, due to its higher initial flow momentum and lower pressure exerted upon the fabric. Interestingly, a more rapid reduction in the required air chamber pressure occurs in the second air chamber than in the first air chamber. This indicates that the pressure of the air fed into the second chamber does not need to be as high as that fed into the first chamber and implies potential energy savings by increasing the cement exit velocity at the hopper stage. Nevertheless, this is only possible if the cement conveying along the ASC does not encounter any severe flow behaviour that impedes its smooth conveyance. To assess that, Fig. 14 shows the streamwise velocity distribution along the ASC where the cement exit velocities are 1m/s and 4m/s, where they are the minimum and maximum exit velocities studied here.

Fig. 14(a) depicts a flow scenario that is more incoherent, due to the low cement exit velocity. Analysis reveals that this is a result of the air issuing from the fabric interacting significantly with the cement flowing along the ASC. As the cement flow velocity reduces, velocity of air passing the fabric becomes relatively more significant and easily perturbs the intended

smoother cement flow down the ASC. Recall from earlier results that interactions between two entities typically lead to vortex formations above the fabric even at a cement exit velocity of 4m/s. When the latter is merely one-quarter of 4m/s, it should not come as a surprise that a more chaotic flow phenomenon is observed here. In practise, such agitated cement flows along the ASC are undesirable, as they meant that higher energy losses will be incurred due to more interactions between the cement and the ASC walls and the conveyance velocity is more than likely to be reduced. A less continuous or even slug flows may develop as a result too. In contrast to Fig. 14(a), Fig. 14(b) shows far less interactions between the cement flow and air issuing from the fabric, thus producing more coherent conveyance flow behaviour. The air passing through the fabric is supporting the cement conveyance down the ASC as it should and potential problems associated with increased flow energy losses and discontinuous cement flows are likely to be significantly less prevalent as well.

It has been postulated during the discussions on Fig. 13 that a faster cement exit velocity from the hopper leads to faster conveyance velocity down the ASC and lower pressure exerted upon the fabric. This is validated in Fig. 15, where the pressure distributions within the ASC are plotted at cement exit velocities of 1m/s and 4m/s. It is clear that a 1m/s cement exit velocity produces significantly higher pressures within the ASC, as compared to those resulting from a 4m/s cement exit velocity. The lower pressures exerted by the cement flow along the ASC at a higher cement exit velocity meant that the fluidized layer between the cement and the fabric is more stable, less likely to break up and more apt in conveying the cement flow down the ASC smoothly.

The preceding results show that increasing the cement exit velocity from the hopper leads to a reduced air chamber pressure requirement, which could possibly reduce the overall energy

consumption of the ASC. Additionally, higher initial cement exit velocity also leads to higher initial flow momentum.

4.4 Effects of suction pressure

Lastly, results pertaining to the effects of suction fan pressure variations will be presented and discussed in this section. For this series of simulations, the operation capacity was kept at C_o=836.68tons/hr, with cement volume fraction of 1 and cement exit velocity from the hopper of 0.6m/s, and only the suction fan pressure was varied.

Fig. 16 plots the variations associated with the first and second air chamber pressure against changes to the suction pressure, based on results obtained from the simulations. It should be reminded that the suction pressure here refers to the induced pressure drop by the suction fan. It can be observed that the required air chamber pressure level reduces as the suction pressure increases, regardless of the exact air chamber. This can be explained by the more dilute phase of cement conveyance down the ASC as the suction pressure increases, which imposes lower pressure requirements for the air using from the fabric to sustain the fluidized bed. Again, this finding can be used to fine-tune the pressure of the air fed into the air chambers, as well as to optimize the suction fan operations for the actual ASC at the operator site.

To better understand the effects of suction pressure changes on the flow characteristics within the cement chamber, Figs. 17 and 18 show the pressure and streamwise velocity distributions along the ASC at 0Pa and 5000Pa suction pressures. Generally speaking, the pressure and velocity distributions are comparable between the two test cases and imply that varying the suction pressure do not introduce noticeable extraneous flow behaviour. From a practical standpoint, employing a larger suction pressure at the end of the ASC may yield better

cement conveyance operations than increasing the pressure of the air fed into the air chambers. The former has been shown to incur little changes to the typical cement conveyance behaviour, while the latter may introduce more interactions between the cement and the supplied air and lead to undesirable cement flow behaviour along the ASC.

To summarize, the suction fan plays an important role in the ASC cement transportation, whereby an increase in the suction pressure enhances the cement conveying rate while incurring less undesirable interactions between cement and air within the ASC system - at least when compared to the effects of varying the air chamber pressure and cement exit velocity.

5. Conclusions

This paper presents results deriving from numerical simulations on the ASC system currently operated by Jurong Port Cement Terminal, Singapore. Based on the physical design, flow conditions and material properties of the ASC at the actual operating site, steady-state simulation of the ASC under current working conditions was firstly carried out.

- Simulation results predicted a declining trend of pressure distribution along the ASC, indicating that pressure gradient and gravitational force are the primary driving forces behind the cement flow.
- Cement particles tend to be located at the lower regions of the cement chamber. The simulations managed to capture strong stochastic and turbulent flow patterns within the ASC system, as well as agreeing well with the cement conveying rate reported by the operator.

Subsequently, steady-state simulations were carried out by varying several key operational parameters, based on a simplified model that included only the first and second cement

chambers. Three key parameters, namely cement mass flow rate, cement exit velocity from the hopper and suction pressure, were studied to explore their impact upon and possible ways to increase cement conveying rate.

- Simulation results indicate that the ASC operation capacity or the cement conveying rate could be improved by increasing air chamber pressure.
- Increasing the cement exit velocity from the hopper leads to a reduced air chamber pressure requirement and possibly reducing the overall energy consumption.
- The suction fan plays an important role in the ASC cement transportation, where increasing the suction pressure enhances the cement conveying rate while incurring less undesirable interactions between cement and air within the ASC system.

Nomenclature

ASC	Air-slide conveyor
C_o	Operation Capacity (tons/hr)
d_p	Particle diameter
$\vec{F}$	Body force
K	Turbulent kinetic energy
k_{eff}	Effective conductivity
L_0	Characteristic dimension of the actual model
$p_{suction}$	Suction pressure (pa)
S_E	Volumetric heat sources
S_t	Stokes number
S_c	Solid concentration
U	Overall Velocity (m/s)
$U_{x,y,z}$	X, Y, Z velocity component (m/s)

U_0	Fluid velocity of flow (m/s)
V_f	Volume fraction of cement
V_{hopper}	Velocity of mixture at hopper (m/s)
v_{fabric}	Velocity of air through fabric (m/s)
$\vec{v}_m$	Mass-averaged velocity
$\vec{v}_{dk}$	Drift velocity for the secondary phase k
β	Incline angle (°)
e	Coefficient of
ρ_p	restitution Particle
ρ_m	density (kg/m^3) Mixture density (kg/m^3)
ρ_{bulk}	Bulk density (kg/m^3)
φ	Particle side (μm)
ε	Turbulent dissipation
σ_k	Volume fraction of phase k
μ_m	Viscosity of the mixture
μ	Air dynamic viscosity

Acknowledgements

The authors gratefully acknowledge the support for the research by Maritime and Port Authority of Singapore and Jurong Port Pte Ltd under a MPA-JP MINT Fund grant, as well as useful technical discussions with MPA and Jurong Port Pte Ltd.

References

1. Cong, X., X. Guo, X. Gong, H. Lu and W. Dong, *Experimental research of flow patterns and pressure signals in horizontal dense phase pneumatic conveying of pulverized coal.* Powder Technology, 2011. **208**(3): p. 600-609.

2. Setia, G. and S.S. Mallick, *Modelling fluidized dense-phase pneumatic conveying of fly ash.* Powder Technology, 2015. **270, Part A**: p. 39-45.
3. Li, K., S.B. Kuang, R.H. Pan and A.B. Yu, *Numerical study of horizontal pneumatic conveying: Effect of material properties.* Powder Technology, 2014. **251**: p. 15-24.
4. Gupta, S.K., V.K. Agarwal, S.N. Singh, V. Seshadri, D. Mills, J. Singh and C. Prakash, *Prediction of minimum fluidization velocity for fine tailings materials.* Powder Technology, 2009. **196**(3): p. 263-271.
5. Yan, F. and A. Rinoshika, *High-speed PIV measurement of particle velocity near the minimum air velocity in a horizontal self-excited pneumatic conveying of using soft fins.* Experimental Thermal and Fluid Science, 2013. **44**: p. 534-543.
6. Gupta, S.K., V.K. Agrawal, S.N. Singh, V. Seshadri and D. Mills, *An experimental investigation on a fluidized motion conveying system.* Powder Technology, 2006. **167**(2): p. 72-84.
7. Mittal, A., S.S. Mallick and P.W. Wypych, *An investigation into pressure fluctuations for fluidized dense-phase pneumatic transport of fine powders.* Powder Technology, 2015. **277**: p. 163-170.
8. Pu, W., C. Zhao, Y. Xiong, C. Liang, X. Chen, P. Lu and C. Fan, *Numerical simulation on dense phase pneumatic conveying of pulverized coal in horizontal pipe at high pressure.* Chemical Engineering Science, 2010. **65**(8): p. 2500-2512.
9. Rinoshika, A., F. Yan and M. Kikuchi, *Experimental study on particle fluctuation velocity of a horizontal pneumatic conveying near the minimum conveying velocity.* International Journal of Multiphase Flow, 2012. **40**: p. 126-135.
10. Breuer, M. and N. Almohammed, *Modeling and simulation of particle agglomeration in turbulent flows using a hard-sphere model with deterministic collision detection and enhanced structure models.* International Journal of Multiphase Flow, 2015. **73**: p. 171-206.
11. Setia, G., S.S. Mallick and P.W. Wypych, *On improving solid friction factor modeling for fluidized dense-phase pneumatic conveying systems.* Powder Technology, 2014. **257**: p. 88-103.
12. Alletto, M. and M. Breuer, *Prediction of turbulent particle-laden flow in horizontal smooth and rough pipes inducing secondary flow.* International Journal of Multiphase Flow, 2013. **55**: p. 80-98.
13. Mason, D.J. and A. Levy, *A model for non-suspension gas–solids flow of fine powders in pipes.* International Journal of Multiphase Flow, 2001. **27**: p. 415-435.
14. Setia, G., S.S. Mallick, R. Pan and P.W. Wypych, *Modeling minimum transport boundary for fluidized dense-phase pneumatic conveying systems.* Powder Technology, 2015. **277**: p. 244-251.
15. Laín, S. and M. Sommerfeld, *Numerical calculation of pneumatic conveying in horizontal channels and pipes: Detailed analysis of conveying behaviour.* International Journal of Multiphase Flow, 2012. **39**: p. 105-120.
16. Liang, C., J.R. Grace, L. Shen, G. Yuan, X. Chen and C. Zhao, *Experimental investigation of pressure letdown flow characteristics in dense-phase pneumatic conveying at high pressure.* Powder Technology, 2015. **277**: p. 171-180.
17. Bareschino, P., R. Solimene, R. Chirone and P. Salatino, *Gas and solid flow patterns in the loop-seal of a circulating fluidized bed.* Powder Technology, 2014. **264**: p. 197-202.
18. Tropea, C., A. Yarin and J.F. Foss, *Springer Handbook of Experimental Fluid Mechanics*2007: Springer. ISBN 978-3-540-25141-5.
19. Mills, D., *Pneumatic conveying design guide*. 2nd ed, pp.70, 2003: Elsevier.

20. Bentz, D.P. and C.J. Haecker, *An argument for using coarse cements in high-performance concretes.* Cement and Concrete Research, 1999. **29**(4): p. 615-618.
21. Bentz, D.P., E.J. Garboczi, C.J. Haecker and O.M. Jensen, *Effects of cement particle size distribution on performance properties of Portland cement-based materials.* Cement and Concrete Research, 1999. **29**(10): p. 1663-1671.
22. Taylor, H.F.W., *Cement Chemistry*. 2nd ed, 1997, London: Thomas Telford.
23. Lefebvre, A. and B. Maury, *Apparent viscosity of a mixture of a Newtonian fluid and interacting particles.* Comptes Rendus Mécanique, 2005. **333**(12): p. 923-933.

Highlights

- An industrial air-slide conveyor was modeled numerically to optimize its operations
- Numerical results agree well with the actual air-slide conveyor conveying capacity
- Effects of hopper exit velocity and suction pressure on cement flow rate are studied
- Increasing air chamber pressure improves cement conveying capacity
- Increasing suction pressure enhances cement conveying operations

Fig. 1
Click here to download high resolution image

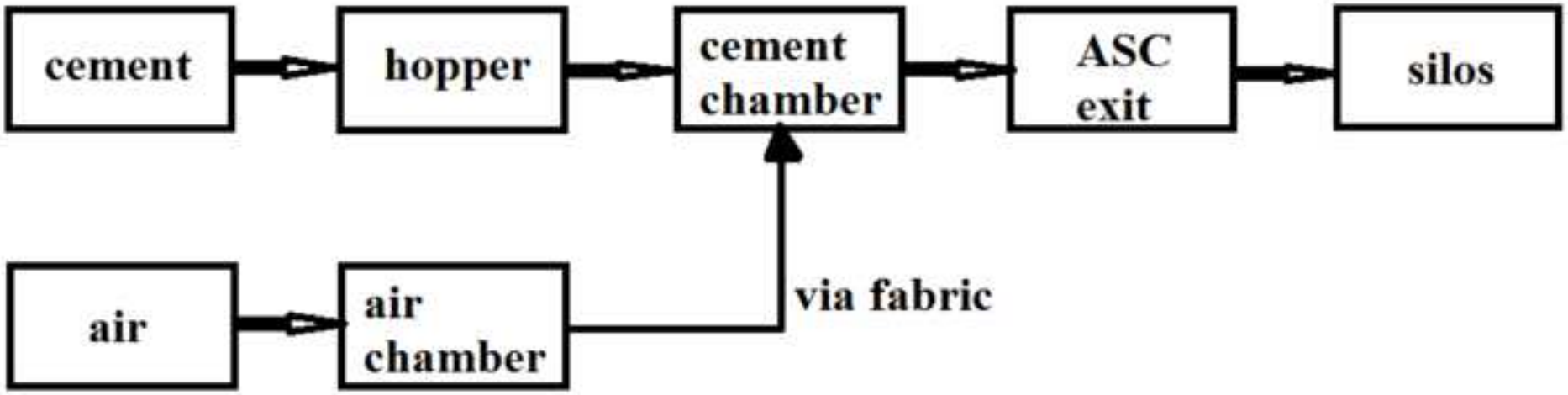

Figure 1 Schematic diagram of the industrial ASC system working process

Fig. 2
Click here to download high resolution image

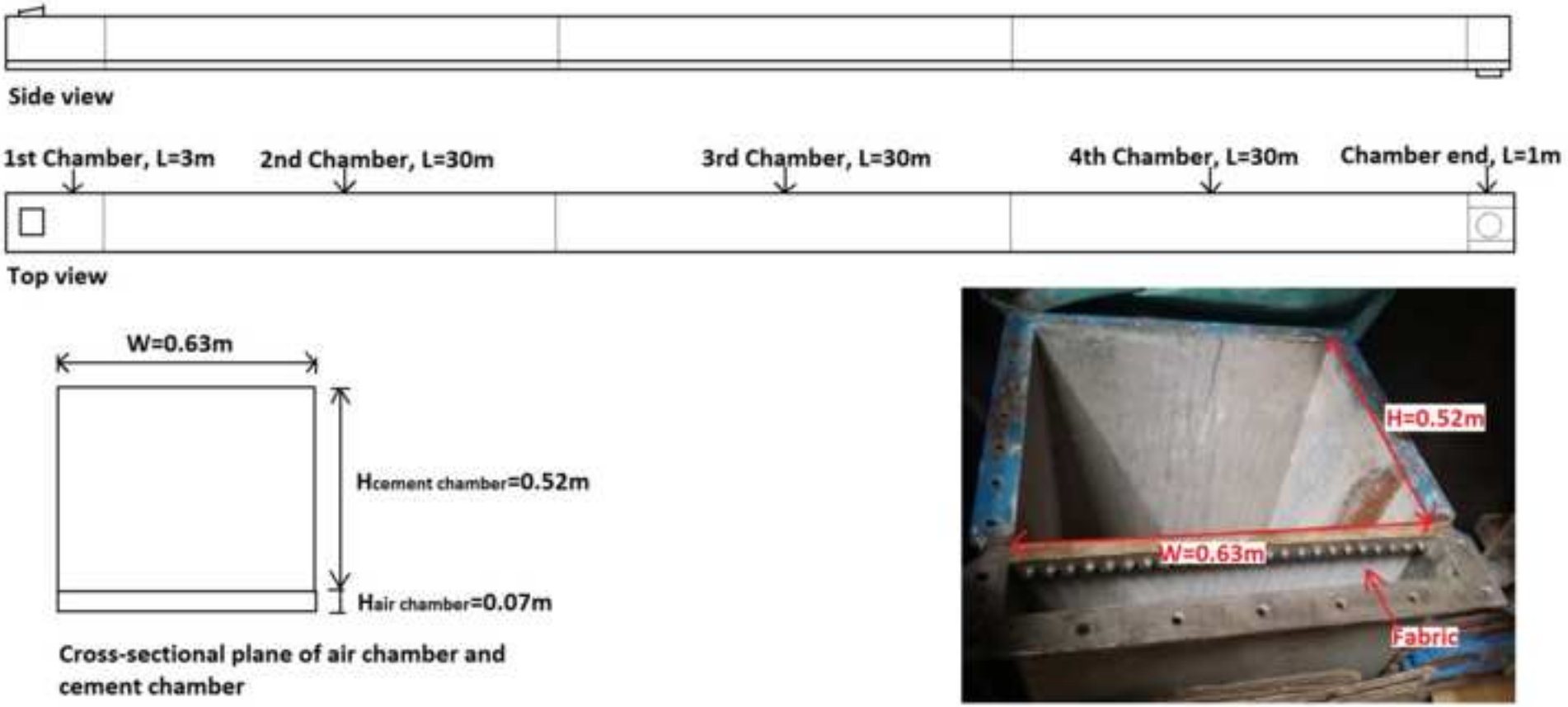

Figure 2 Photo of the actual ASC and its geometrical details

Fig. 3
Click here to download high resolution image

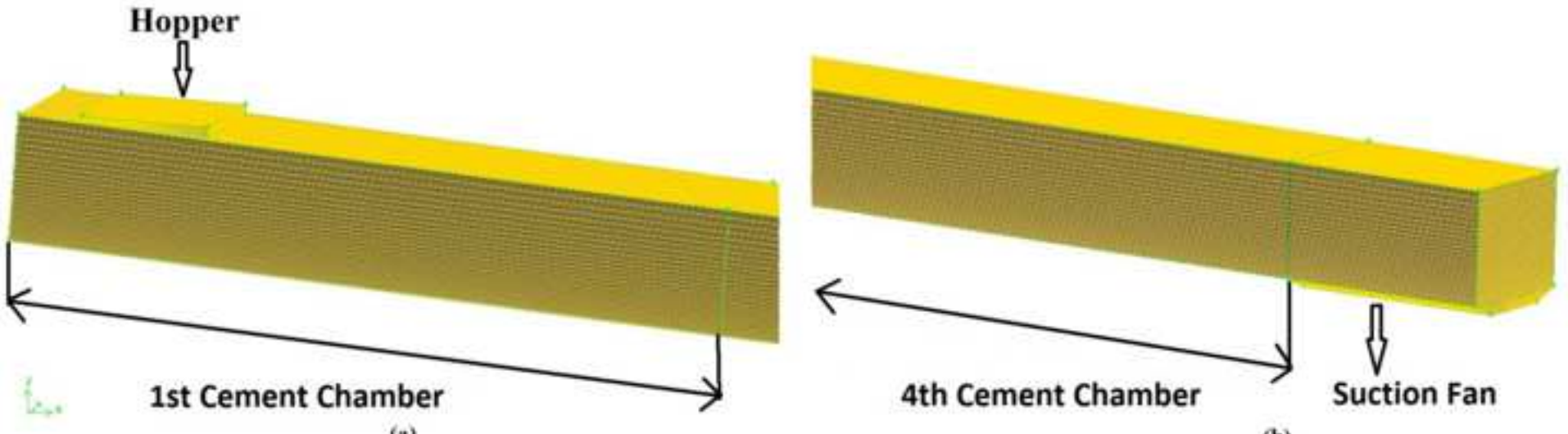

Figure 3 Structured meshes used for (a) hopper exit and first cement chamber and (b) cement chamber end

Fig. 4
Click here to download high resolution image

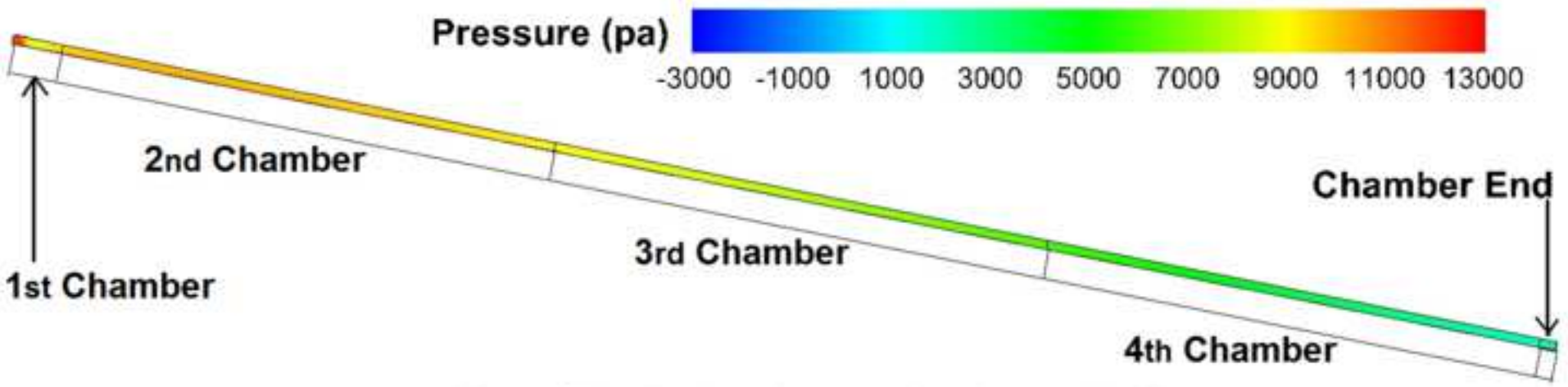

Figure 4 Distribution of pressure along the actual ASC

Fig. 5
Click here to download high resolution image

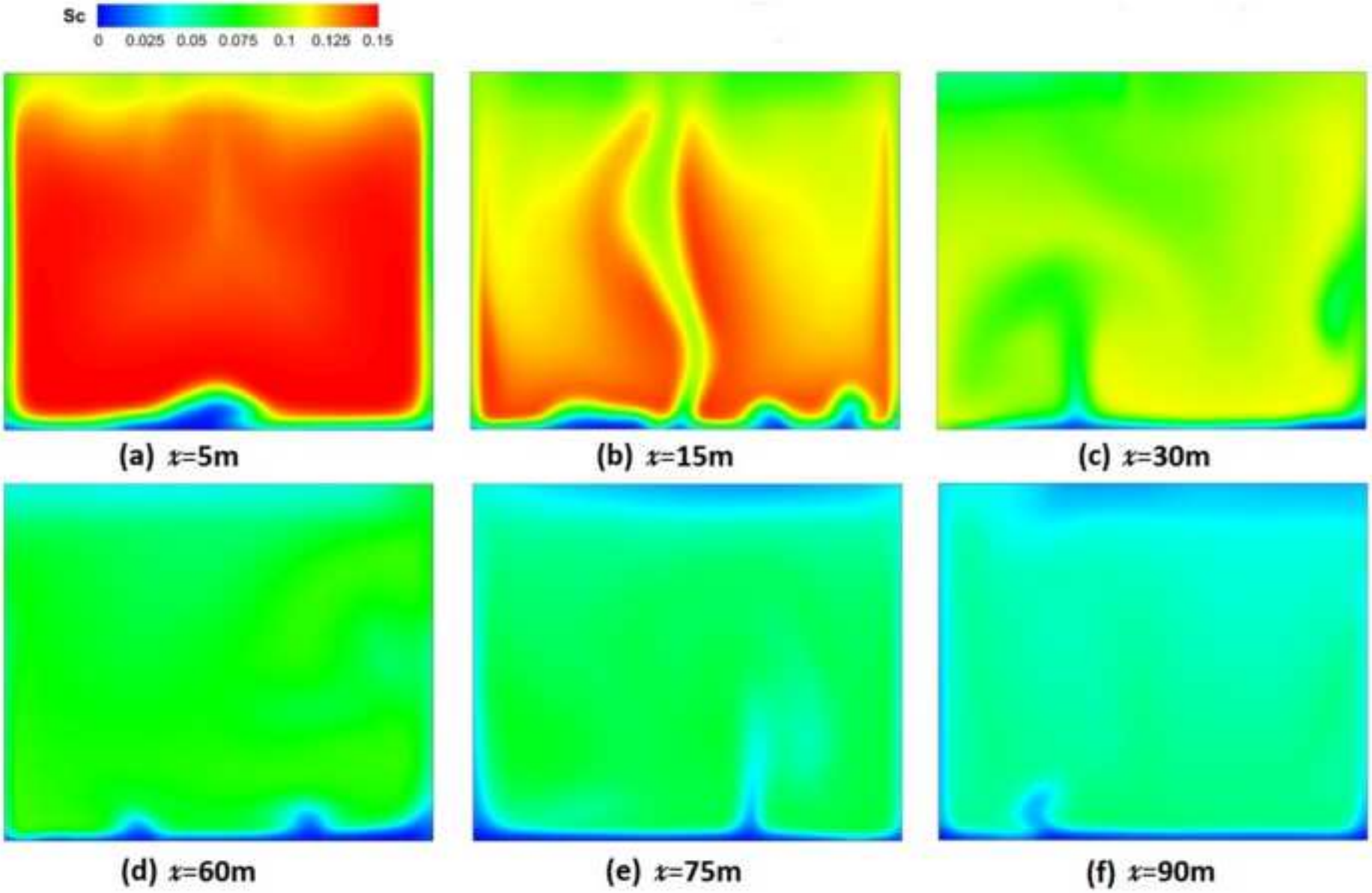

Figure 5 Distributions of solid concentration on different YZ planes

Fig. 6
Click here to download high resolution image

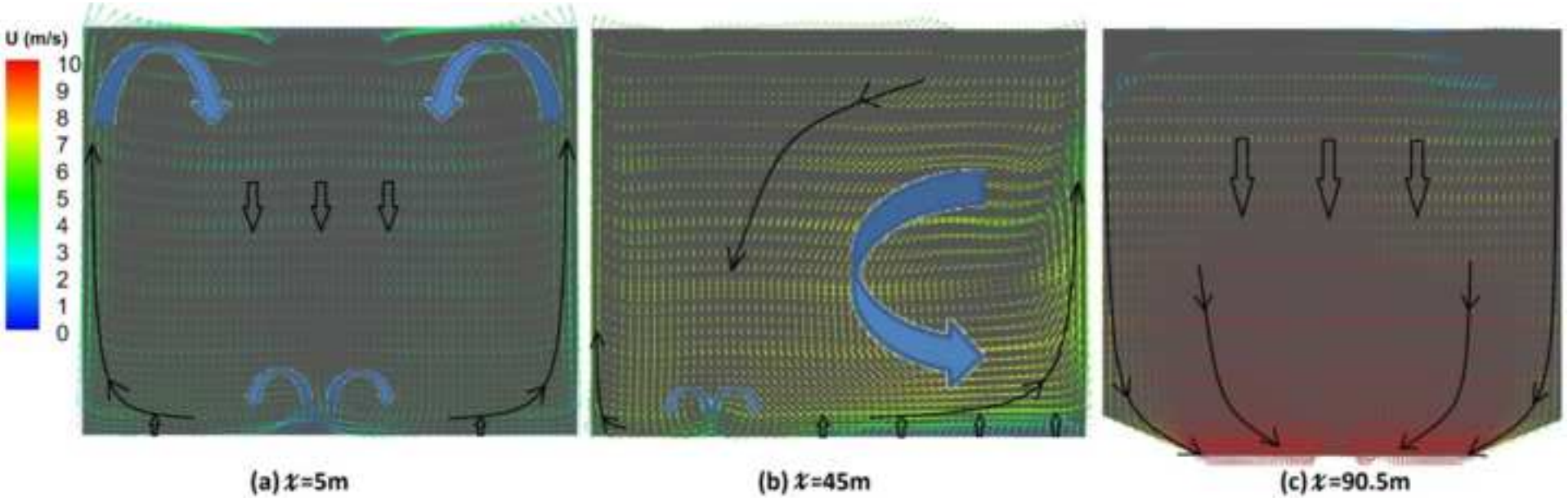

Figure 6 Velocity vector maps along different cross-sectional planes

Fig. 7
Click here to download high resolution image

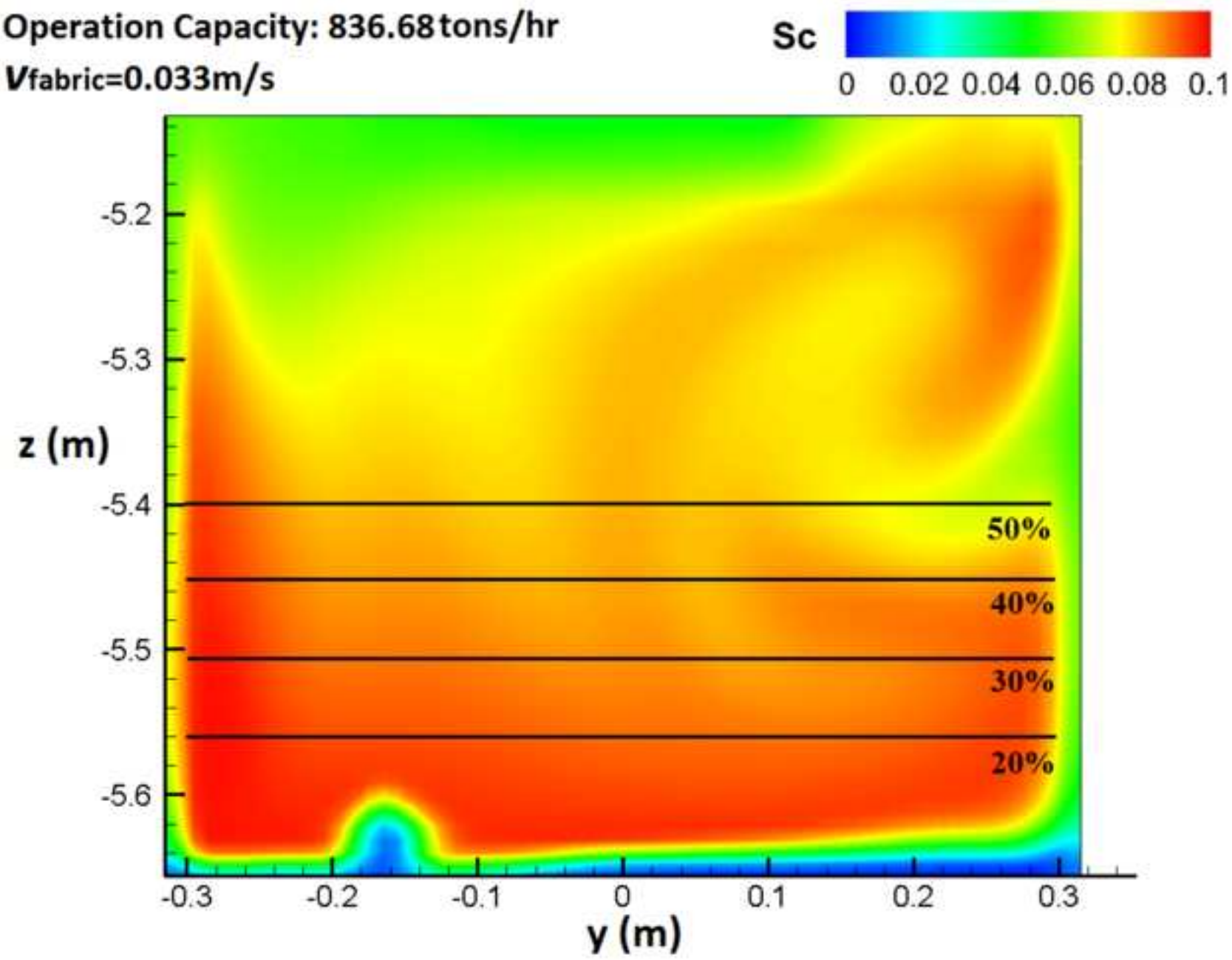

Figure 7 Locations along which solid concentration distributions were extracted along the cross-sectional plane at =45m

Fig. 8

Click here to download high resolution image

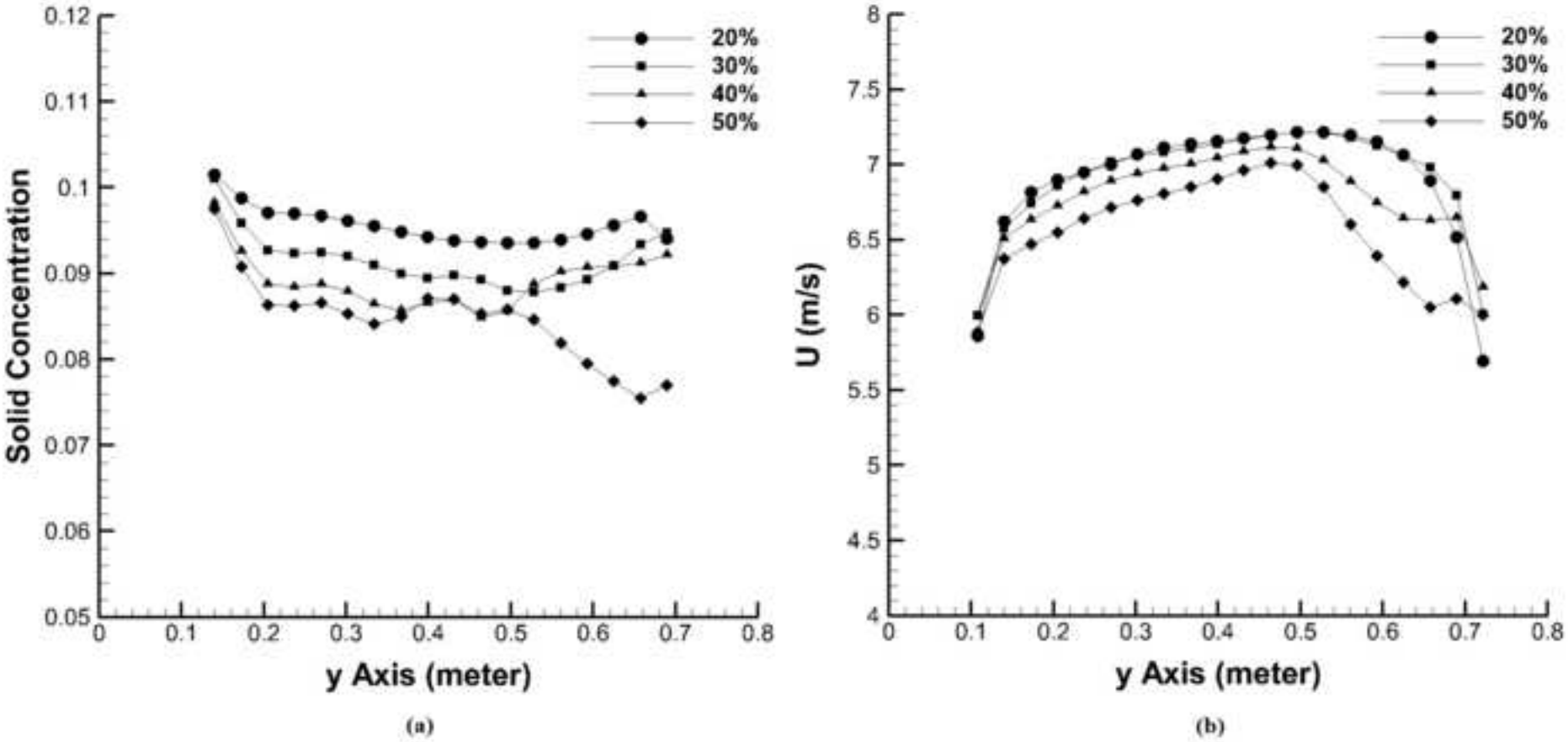

Figure 8 Distributions of (a) solid concentration level and (b) bulk velocity at different distances away from the fabric surface along the cross-sectional plane at =45m.

Fig. 9
Click here to download high resolution image

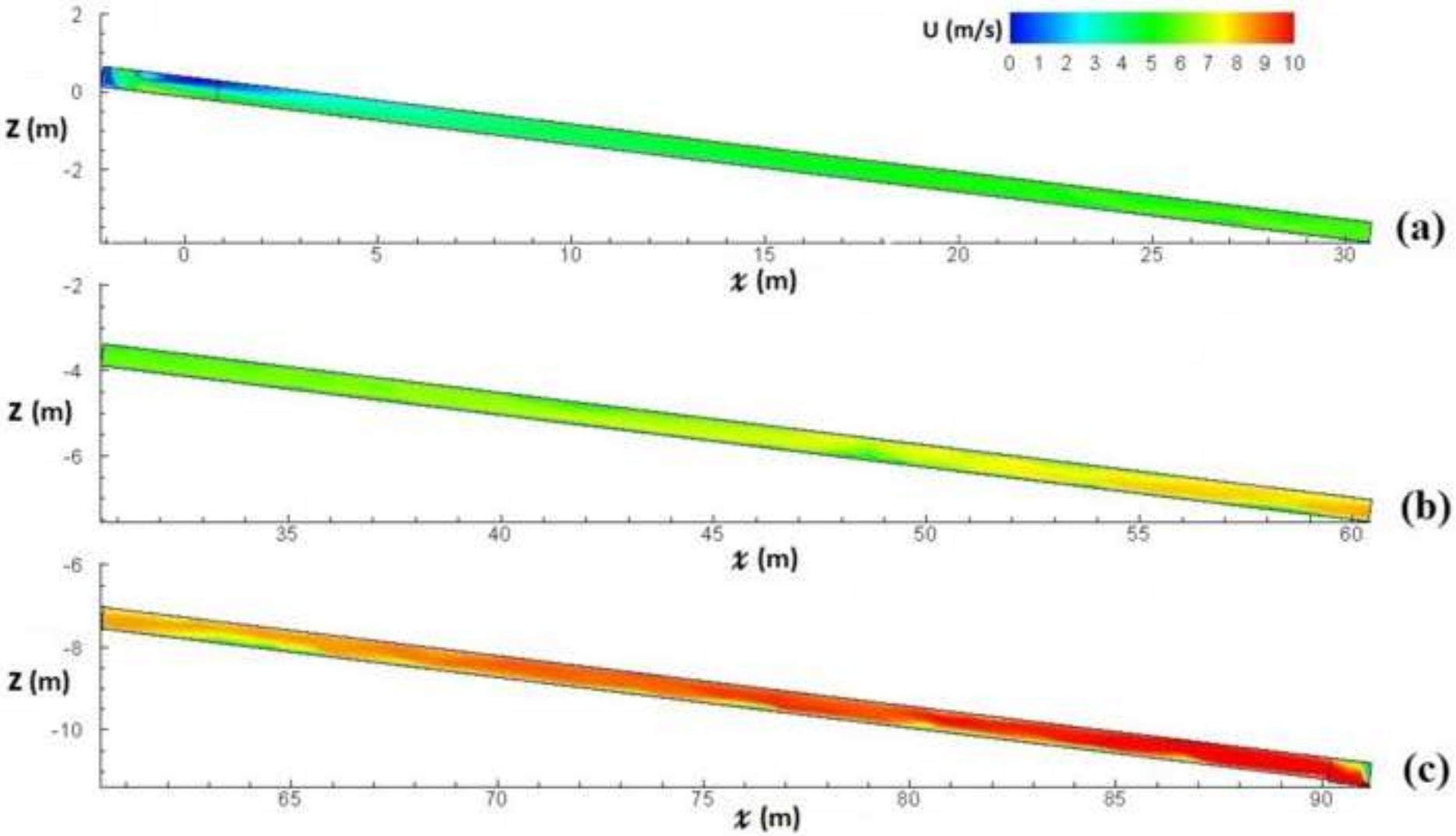

Figure 9 Computed velocity distributions along different sections along the ASC

Fig. 10
Click here to download high resolution image

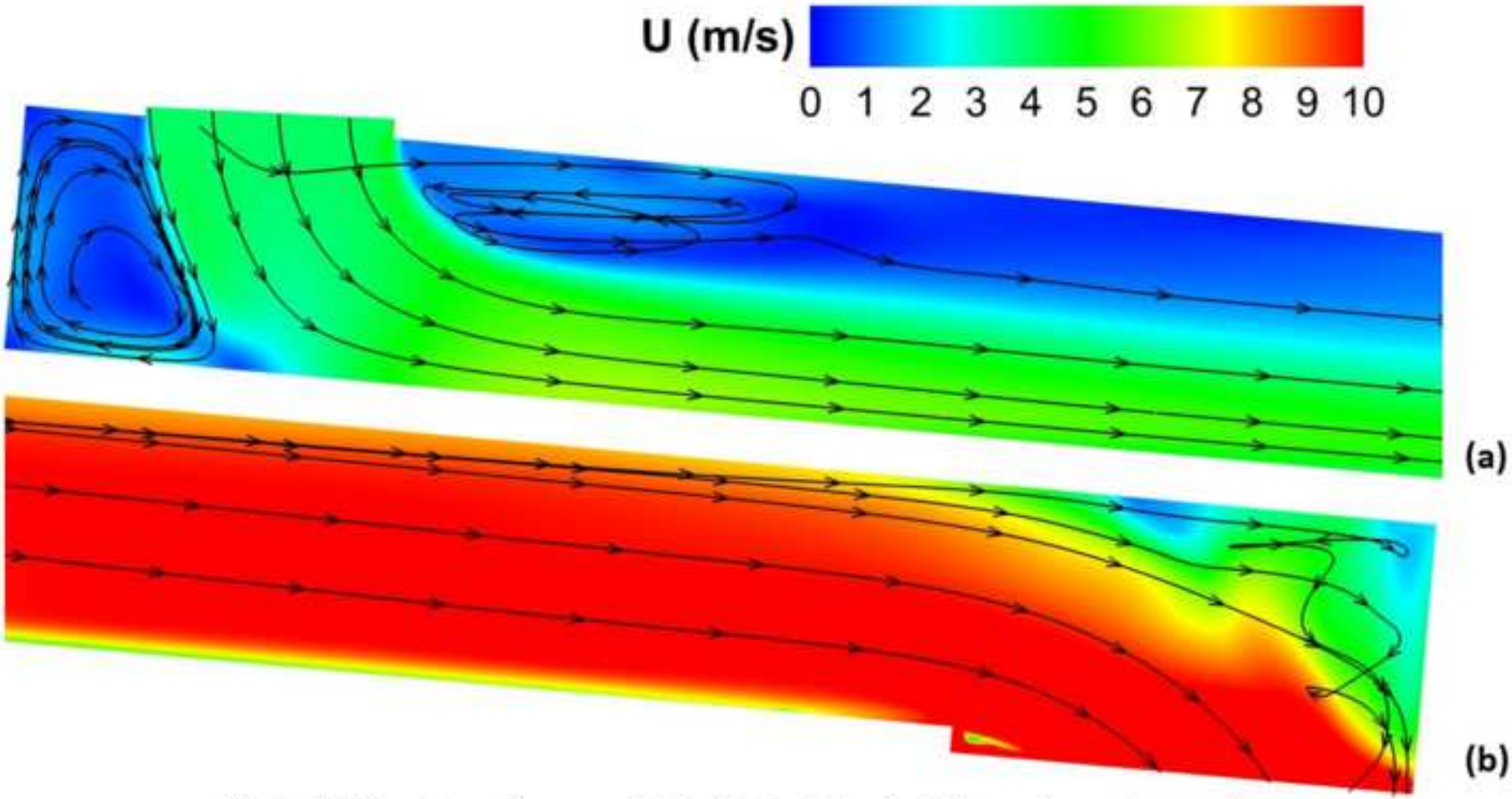

Figure 10 Flow streamlines associated with the (a) recirculating region upstream of the hopper region and (b) flow exiting from the last chamber

Fig. 11
Click here to download high resolution image

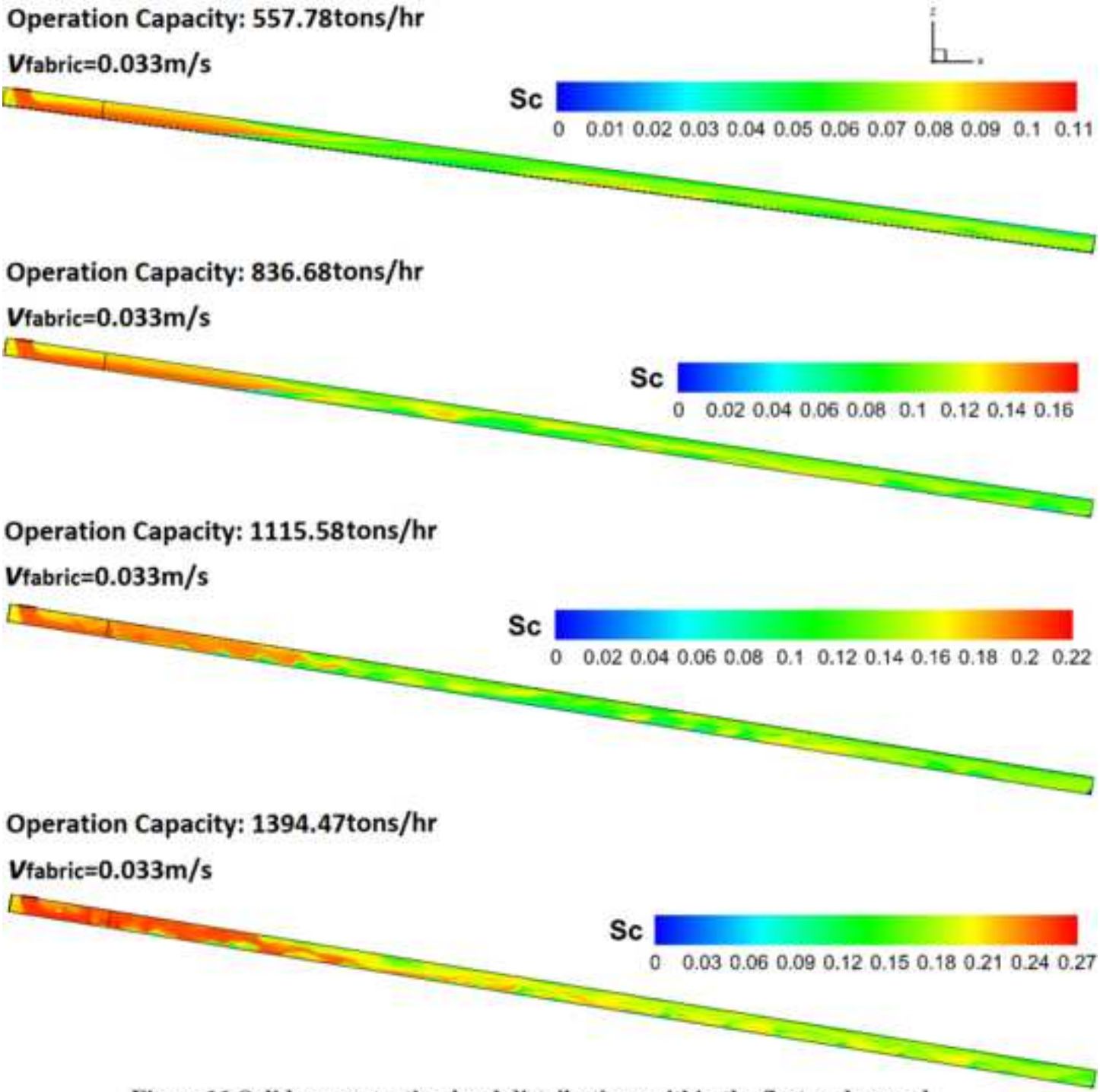

Figure 11 Solid concentration level distributions within the first and second cement chamber associated with different operating capacities

Fig. 12
Click here to download high resolution image

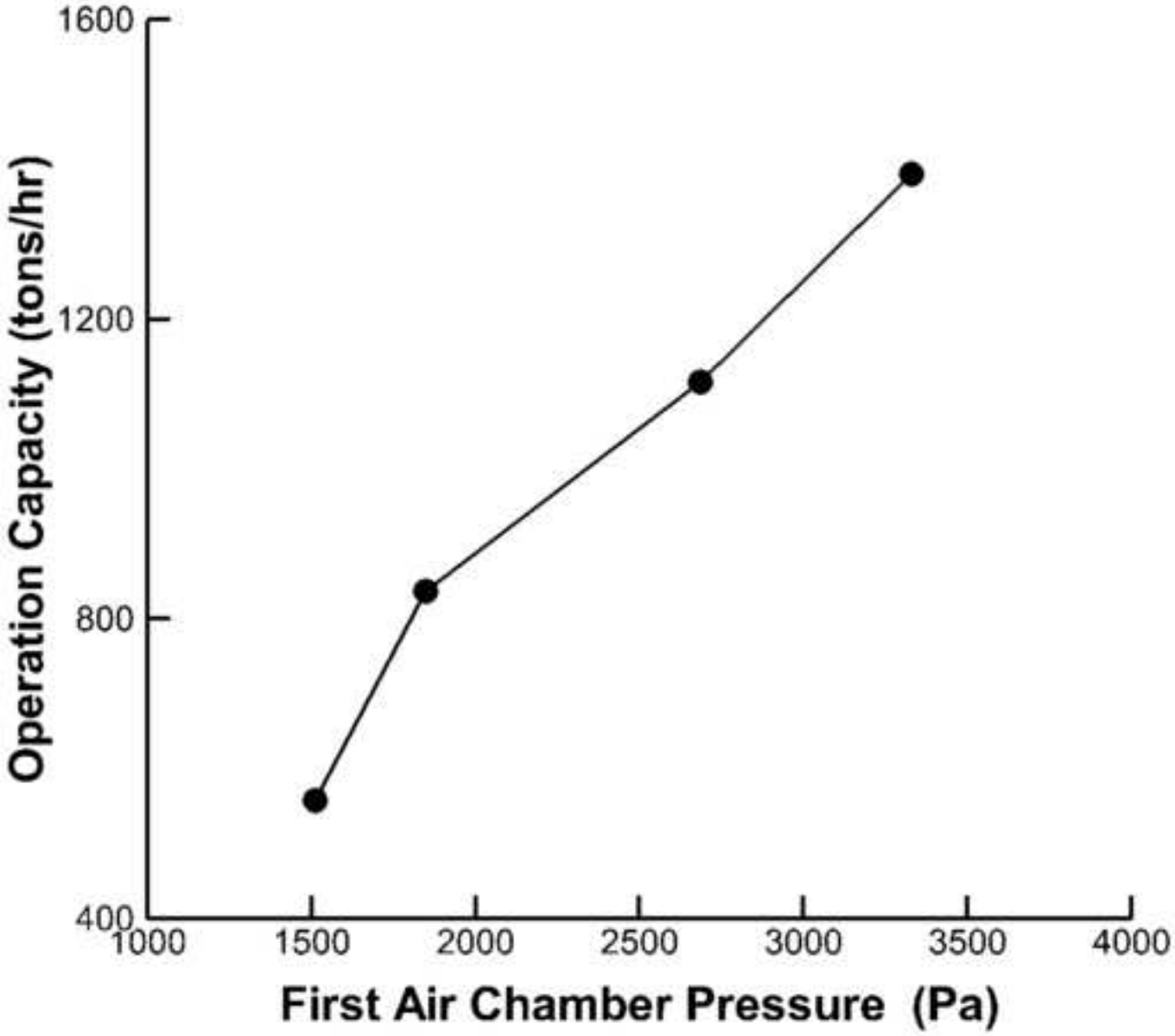

Figure 12 Relationship between the air pressure in first air chamber and operating capacity

Fig. 13
Click here to download high resolution image

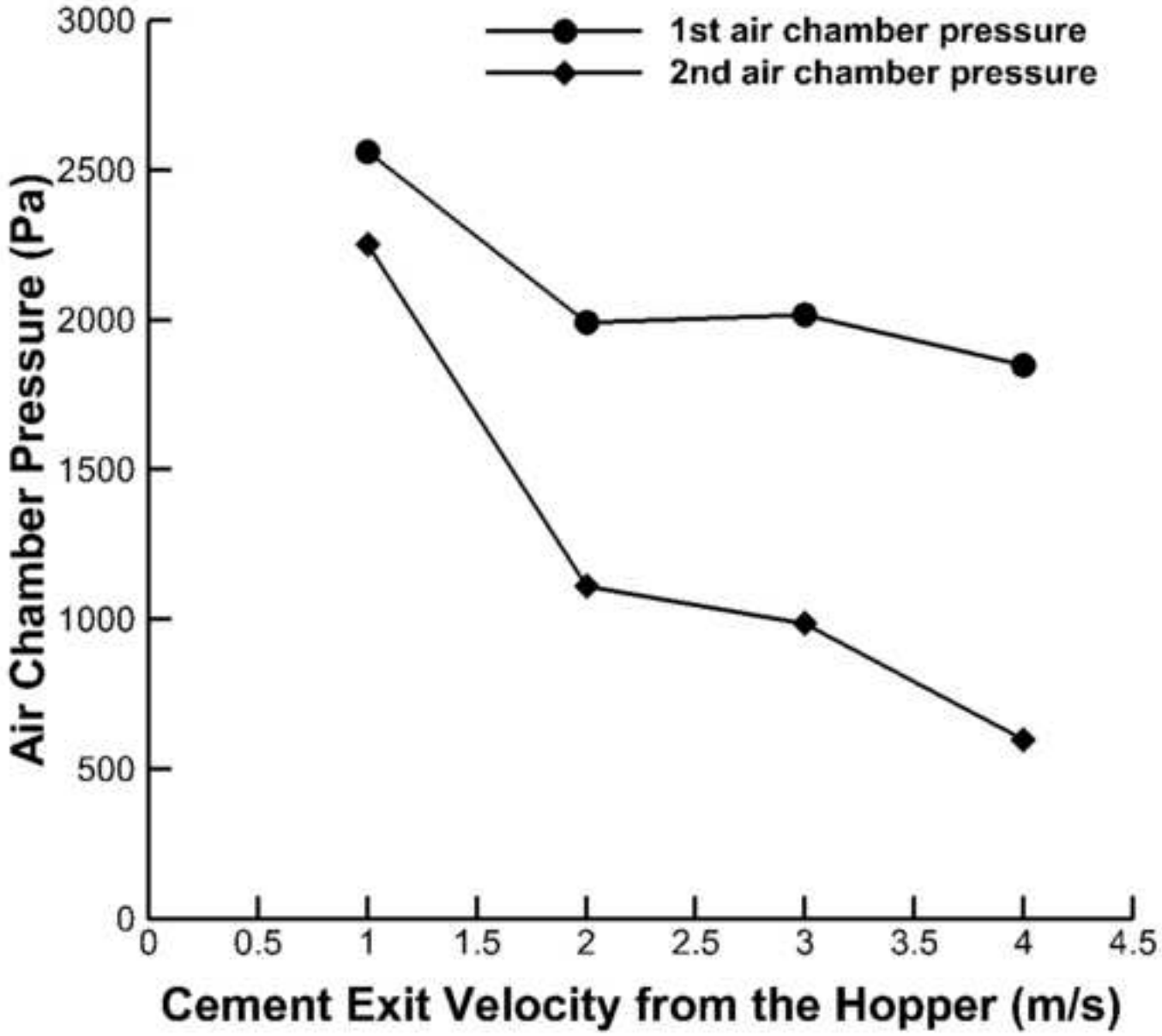

Figure 13 Relationship between the air chamber pressure and cement exit velocity

Fig. 14
Click here to download high resolution image

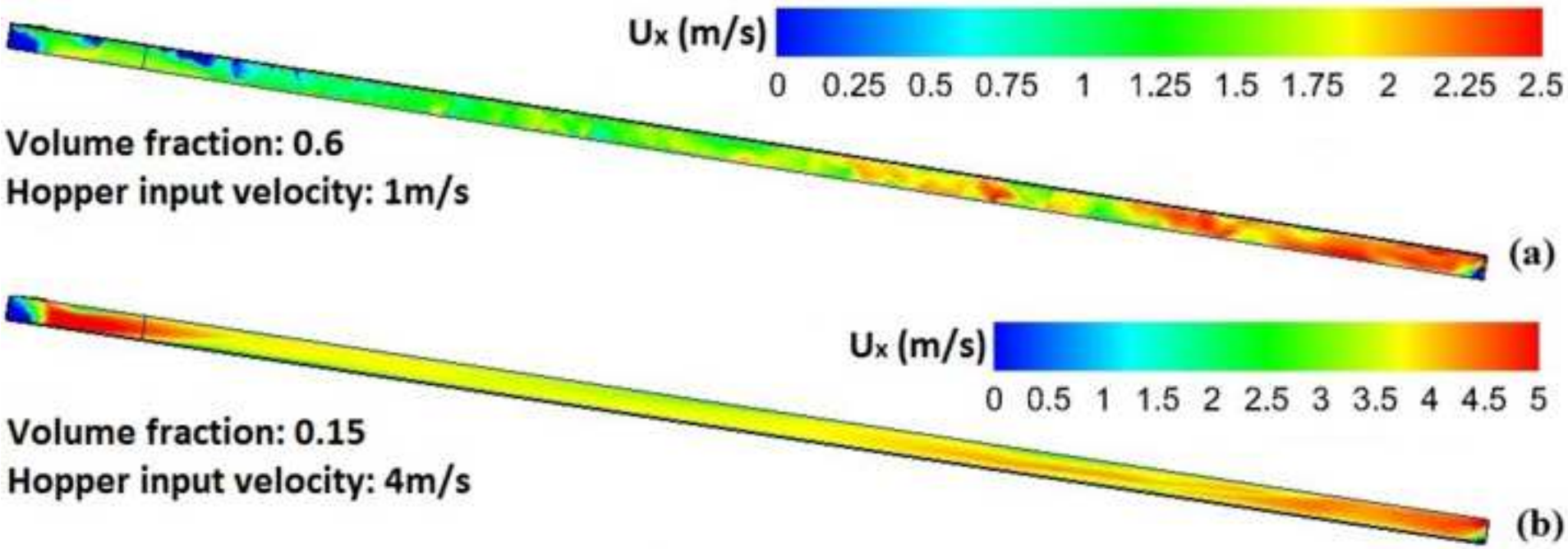

Figure 14 Streamwise velocity distributions along the ASC system for cement exit velocities of (a) 1m/s and (b) 4m/s

Fig. 15
Click here to download high resolution image

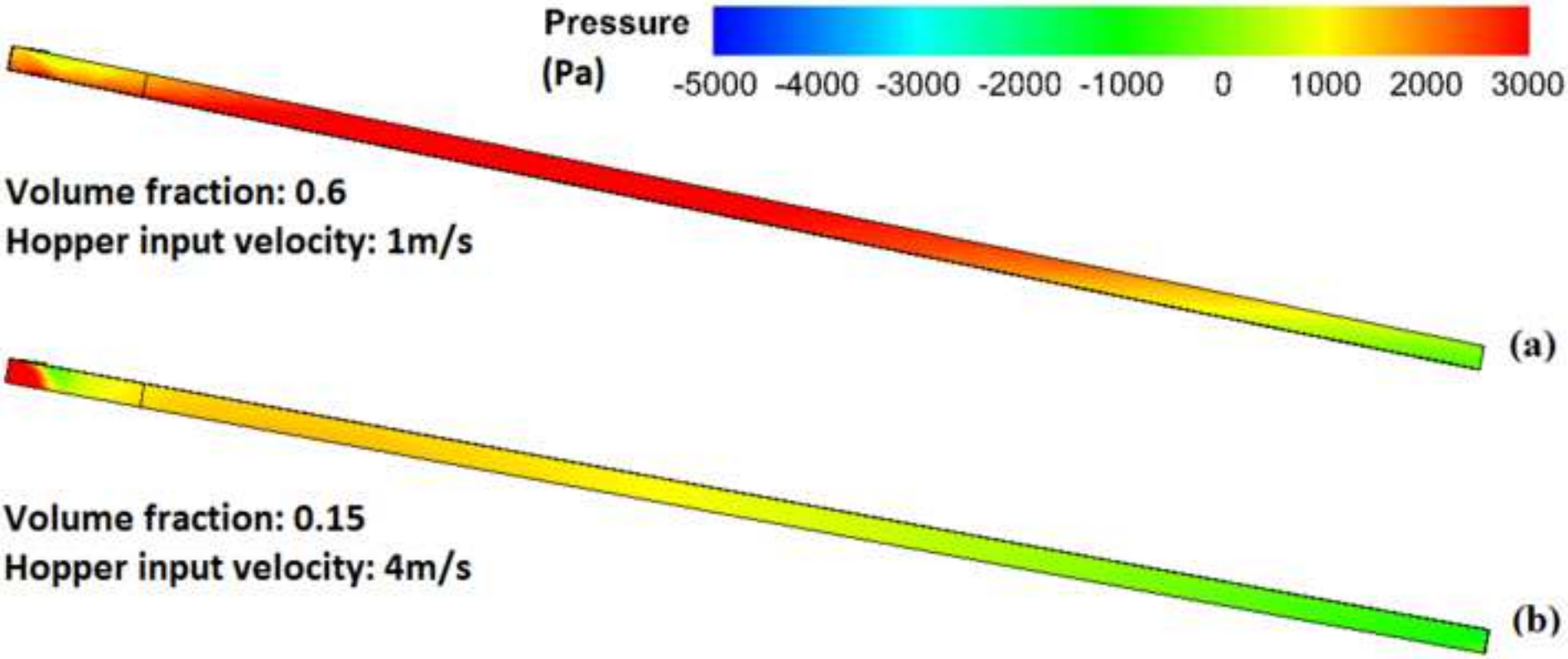

Figure 15 Pressure distributions along the ASC system for cement exit velocities of (a) 1m/s and (b) 4m/s

Fig. 16
Click here to download high resolution image

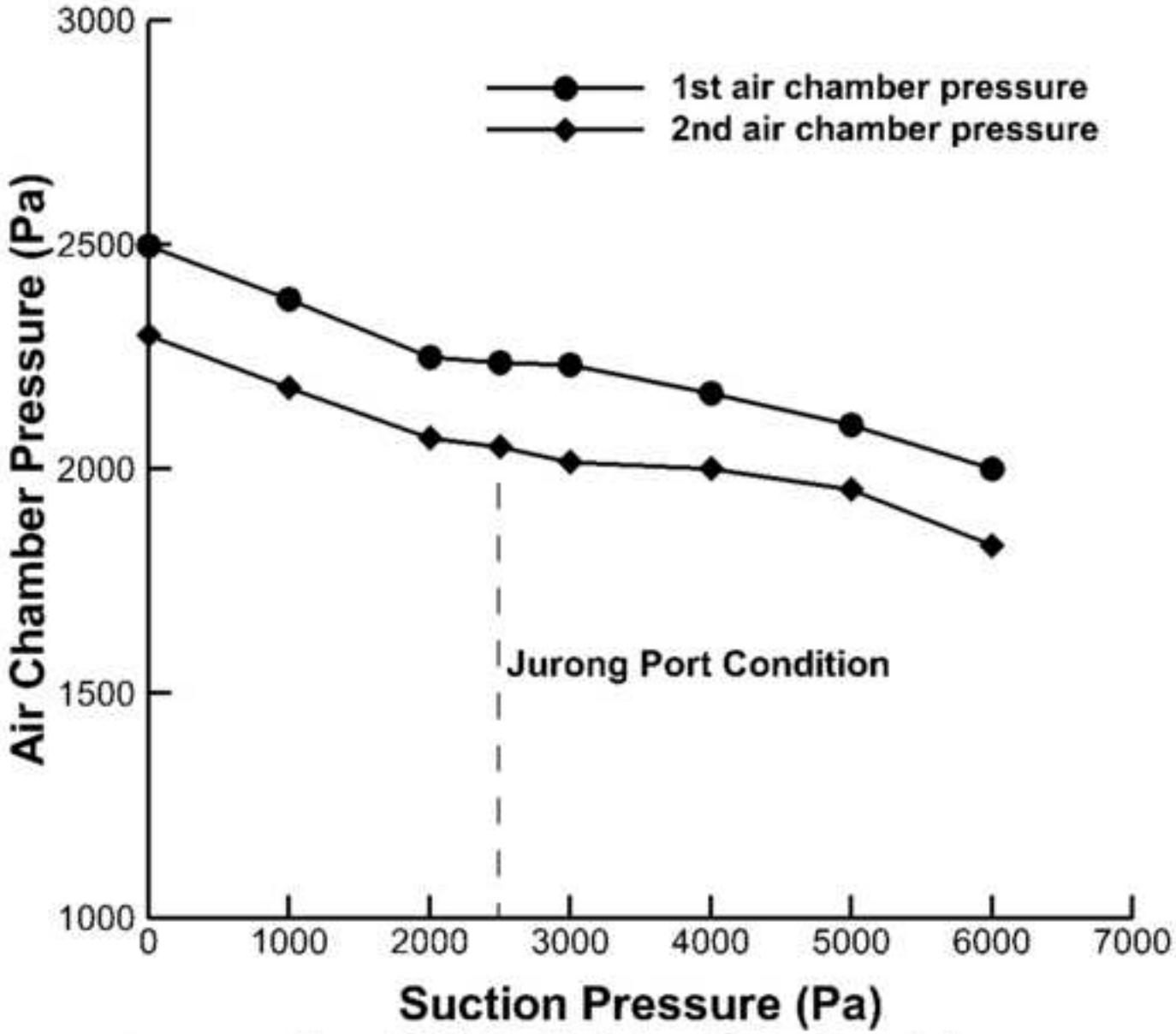

Figure 16 Relationships between first and second air chamber pressure with suction pressure variations

Fig. 17
Click here to download high resolution image

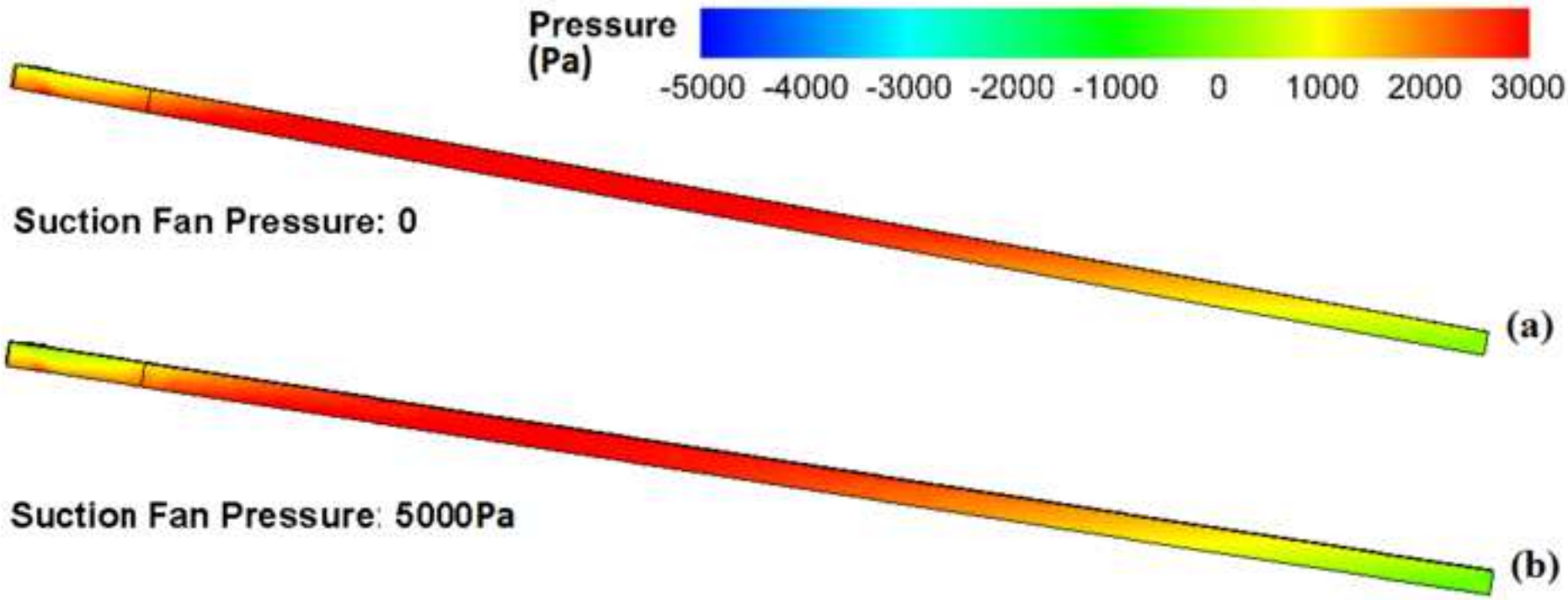

Figure 17 Pressure distributions associated with (a) 0Pa and (b) 5000Pa suction pressures

Fig. 18
Click here to download high resolution image

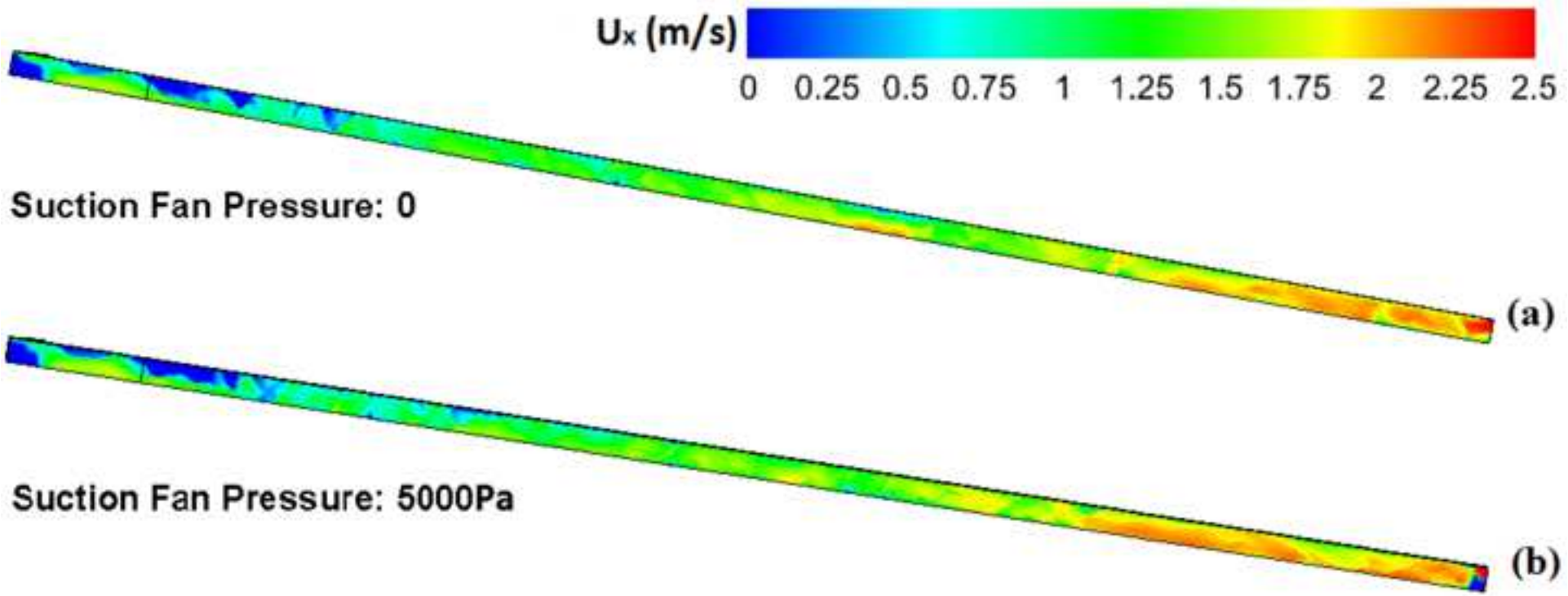

Figure 18 Streamwise velocity distributions associated with (a) 0Pa and (b) 5000Pa suction pressures

Table 1
Click here to download high resolution image

Table 1 Design and Operation Details of the ASC

Total length	94m
Width	0.63m
Height of cement chamber	0.52m
Height of air chamber	0.07m
Conveyor inclination	7°
Number of air-injection points	4
First air chamber length	3.012m
Second, third and fourth air chamber length	30m (per chamber)
First air chamber pressure	7500Pa
Second, third and fourth air chamber pressure	6000Pa
Suction fan pressure drop, $p_{suction}$	2500Pa
Operation capacity, C_o	800tons/hr
Air velocity through fabric, v_{fabric}	0.033m/s

Table 2 Input parameters for simulations

Fluid material type	Air
Granule material type	Cement Portland
Mean cement particle size	14μm
Bulk density	1362kg/m^3
Conveyor inclination	7°
Air velocity through fabric	0.033m/s
Hopper area	0.2844m^2
Mixture velocity at hopper	4m/s
Volume fraction of cement at hopper	0.15
Suction fan pressure drop	2500Pa
Operation capacity	836.68tons/hr

Table 3

Table 3 Cement mass flow rates and operation capacities associated with different cement volume fractions

Volume fraction of cement	Bulk density (kg/m^3)	Hopper velocity (m/s)	Hopper area (m^2)	Mass flow rate (kg/s)	Operation capacity (tons/hr)
0.1	1362	4	0.2844	154.94	557.78
0.15	1362	4	0.2844	232.41	836.68
0.2	1362	4	0.2844	309.88	1115.58
0.25	1362	4	0.2844	387.35	1394.47

Table 4
Click here to download high resolution image

Table 4 Change of combination of input parameters

Volume fraction of cement	Fluidized density (kg/m^3)	Hopper velocity (m/s)	Hopper area (m^2)	Mass flow rate (kg/s)	Operation capacity (tons/hr)
0.6	817.2	1	0.2844	232.41	836.68
0.3	408.6	2	0.2844	234.41	836.68
0.2	272.4	3	0.2844	234.41	836.68
0.15	204.3	4	0.2844	234.41	836.68